Control Engineering Practice 141 (2023) 105694

Contents lists available at ScienceDirect

Control Engineering Practice

journal homepage: www.elsevier.com/locate/conengprac

Multirate feedforward control with mode decomposition for intersample performance in multivariable motion systems

Masahiro Mae *, Wataru Ohnishi, Hiroshi Fujimoto

The University of Tokyo, 5-1-5, Kashiwanoha, Kashiwa, Chiba, 277-8561, Japan

ARTICLE INFO

Keywords:
Multirate feedforward control
Perfect tracking control
Zero-order-hold
Mode decomposition
Intersample performance

ABSTRACT

Multirate feedforward control enables perfect tracking control for the desired state trajectory at every sample as the same number of the model order. The aim of this paper is the comparison of perfect tracking control approaches for intersample performance in multi-modal motion systems. The multirate feedforward control has a trade-off between the number of states for perfect tracking control and the reference sampling frequency. To balance the trade-off, the states for the perfect tracking control can be selected by the mode decomposition. Intersample performance of each approach in a multi-modal motion system is compared in both frequency domain and time domain.

1. Introduction

Feedforward control based on exact model inversion enables perfect tracking control (Tomizuka, 1987) for the model of the controlled system. The quality of the feedforward controller directly results in tracking performance in high-precision mechatronic systems such as wafer scanners (Steinbuch, Oomen, & Vermeulen, 2021), wire bonders (Poot, Portegies, Mooren, van Haren, van Meer, & Oomen, 2022), and ball-screw-driven stages (Hayashi, Fujimoto, Isaoka, & Terada, 2020). In industrial applications, the system is controlled in discrete time but the tracking performance should be improved in continuous time.

The exact model inversion has a challenge when the model has nonminimum-phase zeros such as intrinsic and discretization zeros (Åström, Hagander, & Sternby, 1984). Several approximated inverse approaches include zero-phase-error tracking control (ZPETC) (Tomizuka, 1987), nonminimum-phase zeros ignore (NPZI) (Gross, Tomizuka, & Messner, 1994), and zero-magnitude-error tracking controller (ZMETC) method (Wen & Potsaid, 2004), and comparisons are provided in Butterworth, Pao, and Abramovitch (2012), van Zundert and Oomen (2018). These approaches cannot provide exact on-sample tracking due to approximation. The single-rate stable inversion approach (van Zundert & Oomen, 2018) generates the noncausal bounded feedforward input for the model with nonminimum-phase zeros and provides perfect output tracking for every sample. However, it cannot compensate for the zeros around -1 of the discrete-time model that cause the oscillating feedforward input and deteriorate intersample performance when the relative degree of the continuous-time model is 2 or more (Åström et al., 1984).

To improve intersample performance, the multirate feedforward control (Fujimoto, Hori, & Kawamura, 2001; Ohnishi, Beauduin, & Fujimoto, 2019) is presented. The multirate feedforward control provides perfect n states tracking for every n sample and prevents intersample oscillation. There is a trade-off in the multirate feedforward control between the number of states for perfect tracking control and the reference sampling frequency. To balance the trade-off, the multirate feedforward control approaches based on modal form with additive decomposition (Mae, Ohnishi, & Fujimoto, 2021; Ohnishi & Fujimoto, 2018) and multiplicative decomposition (van Zundert, Ohnishi, Fujimoto, & Oomen, 2020) are presented. Both approaches select the states for perfect tracking control and balance the trade-off to improve intersample performance. Note that the concept of perfect tracking control is defined in the sampled-data controlled systems as "the output perfectly tracks the reference with zero tracking error at every sampling point" (Tomizuka, 1987). The concept of perfect tracking control is in discrete time, and it is distinguished from the concept of perfect control in continuous time (Skogestad & Postlethwaite, 2005).

There are other finite sample preview feedforward control approaches (Duan, Yoon, & Okwudire, 2018; Hirata & Ueno, 2011; Totani & Nishimura, 1994) based on minimizing the two-norm of the tracking error with optimization or least square calculation. These approaches can deal with constraints using the redundancy of the preview samples. However, these concepts are not the same as the exact model inversion approaches such as the single-rate stable inversion and the multirate feedforward control which provide exact on-sample tracking for the model, and the number of preview samples is normally larger than that of the exact model inversion approaches.

* Corresponding author.
E-mail address: mmae@ieee.org (M. Mae).

https://doi.org/10.1016/j.conengprac.2023.105694
Received 24 March 2023; Received in revised form 31 July 2023; Accepted 5 September 2023

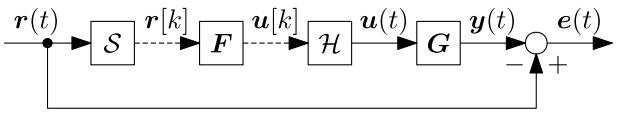

Fig. 1. Block diagram of tracking control. The continuous-time system $\boldsymbol{G}$ is controlled by the discrete-time controller $\boldsymbol{F}$ with sampler $\mathcal{S}$ and zero-order-hold $\mathcal{H}$. The objective is to minimize the continuous-time error $\boldsymbol{e}(t)$.

Although several approaches are available to design the perfect tracking controller, the choice of the feedforward controller can be arbitrarily and there is no comparison in terms of intersample performance for perfect tracking controllers. The aim of this paper is the analysis of pre-existing perfect tracking controllers in both frequency domain and time domain and provides the guideline to design the feedforward controller to improve intersample performance. The main contributions of this paper are as follows.

Contribution 1. *Perfect tracking control approaches are described focusing on improving intersample performance in multi-modal motion systems.*

Contribution 2. *Intersample performance of each approach is evaluated in both frequency domain and time domain.*

The theory is described in a general multi-input multi-output (MIMO) system and the verification is conducted in a single-input single-output (SISO) system.

The outline is as follows. In Section 2, the tracking problem for intersample performance is formulated. In Section 3, the desired state trajectory generation method is presented for SISO and MIMO systems. In Section 4, the multirate feedforward controller design methods with additive and multiplicative decomposition are presented. In Section 5, the intersample performance is validated in a multi-modal motion system. In Section 6, conclusions are presented.

2. Problem formulation

In this section, the problem to improve continuous-time tracking performance is formulated. The perfect tracking control methods based on the single-rate and multirate feedforward are described. From the trade-off of these two approaches, the requirements of the optimal perfect tracking controller design are presented.

2.1. Intersample performance in sampled-data control

The considered tracking control configuration is shown in Fig. 1, with input $\boldsymbol{u} \in \mathbb{R}^{n_u}$, output $\boldsymbol{y} \in \mathbb{R}^{n_y}$, reference $\boldsymbol{r} \in \mathbb{R}^{n_y}$, and error $\boldsymbol{e} \in \mathbb{R}^{n_y}$. In this paper, the system is assumed to be square as $n_u = n_y = m$. The m-input m-output n^{th} order continuous-time linear time-invariant system $\boldsymbol{G}_c \overset{s}{=} (\boldsymbol{A}_c, \boldsymbol{B}_c, \boldsymbol{C}_c, \boldsymbol{O})$ is given by

$$\dot{\boldsymbol{x}}(t) = \boldsymbol{A}_c \boldsymbol{x}(t) + \boldsymbol{B}_c \boldsymbol{u}(t), \tag{1}$$

$$\boldsymbol{y}(t) = \boldsymbol{C}_c \boldsymbol{x}(t), \tag{2}$$

where $\boldsymbol{A}_c \in \mathbb{R}^{n\times n}$, $\boldsymbol{B}_c \in \mathbb{R}^{n\times m}$, and $\boldsymbol{C}_c \in \mathbb{R}^{m\times n}$. The discrete-time system $\boldsymbol{H}_d$ of the continuous-time system $\boldsymbol{H}_c$ discretized by sampler $\mathcal{S}$ and zero-order-hold $\mathcal{H}$ in sampling time δ is generally defined as

$$\boldsymbol{H}_c \overset{s}{=} \left[\begin{array}{c|c} \boldsymbol{A}_c & \boldsymbol{B}_c \\ \hline \boldsymbol{C}_c & \boldsymbol{D}_c \end{array}\right], \tag{3}$$

$$\boldsymbol{H}_d \overset{z}{=} \mathcal{S}\boldsymbol{H}_c\mathcal{H} = \left[\begin{array}{c|c} \boldsymbol{A}_d & \boldsymbol{B}_d \\ \hline \boldsymbol{C}_d & \boldsymbol{D}_d \end{array}\right] = \left[\begin{array}{c|c} e^{\boldsymbol{A}_c\delta} & \boldsymbol{A}_c^{-1}(e^{\boldsymbol{A}_c\delta} - \boldsymbol{I})\boldsymbol{B}_c \\ \hline \boldsymbol{C}_c & \boldsymbol{D}_c \end{array}\right], \tag{4}$$

$$\boldsymbol{x}[k] = \boldsymbol{x}(k\delta). \tag{5}$$

The discrete-time system $\boldsymbol{G}_d \overset{z}{=} (\boldsymbol{A}_d, \boldsymbol{B}_d, \boldsymbol{C}_d, \boldsymbol{O}) = \mathcal{S}\boldsymbol{G}_c\mathcal{H}$ is given by

$$\boldsymbol{x}[k+1] = \boldsymbol{A}_d \boldsymbol{x}[k] + \boldsymbol{B}_d \boldsymbol{u}[k], \tag{6}$$

$$\boldsymbol{y}[k] = \boldsymbol{C}_d \boldsymbol{x}[k]. \tag{7}$$

The control objective considered in this paper is to minimize the continuous-time error $\boldsymbol{e}(t)$ that includes both on-sample and intersample performance for the continuous-time reference $\boldsymbol{r}(t)$ that is assumed to be known in advance.

2.2. Single-rate feedforward control based on discrete-time model inversion

The one-sample forward shifted system $\tilde{\boldsymbol{G}}_d$ of $\boldsymbol{G}_d$ from $\boldsymbol{u}[k]$ to $\boldsymbol{y}[k+1]$ is given by

$$\boldsymbol{x}[k+1] = \boldsymbol{A}_d \boldsymbol{x}[k] + \boldsymbol{B}_d \boldsymbol{u}[k], \tag{8}$$

$$\boldsymbol{y}[k+1] = \boldsymbol{C}_d \boldsymbol{A}_d \boldsymbol{x}[k] + \boldsymbol{C}_d \boldsymbol{B}_d \boldsymbol{u}[k]. \tag{9}$$

For the system $\boldsymbol{H} = (\boldsymbol{A}, \boldsymbol{B}, \boldsymbol{C}, \boldsymbol{D})$ with nonsingular $\boldsymbol{D}$, the inverse system $\boldsymbol{H}^{-1}$ is generally defined as

$$\boldsymbol{H}^{-1} = \left[\begin{array}{c|c} \boldsymbol{A} - \boldsymbol{B}\boldsymbol{D}^{-1}\boldsymbol{C} & \boldsymbol{B}\boldsymbol{D}^{-1} \\ \hline -\boldsymbol{D}^{-1}\boldsymbol{C} & \boldsymbol{D}^{-1} \end{array}\right]. \tag{10}$$

By inverting $\tilde{\boldsymbol{G}}_d$, the input $\boldsymbol{u}$ generated by the single-rate feedforward controller is given by

$$\boldsymbol{u}[k] = \tilde{\boldsymbol{G}}_d^{-1} \boldsymbol{r}[k+1], \tag{11}$$

where the single-rate feedforward controller $\tilde{\boldsymbol{G}}_d^{-1}$ is given by

$$\tilde{\boldsymbol{G}}_d^{-1} = \left[\begin{array}{c|c} \boldsymbol{A}_d - \boldsymbol{B}_d(\boldsymbol{C}_d\boldsymbol{B}_d)^{-1}\boldsymbol{C}_d\boldsymbol{A}_d & \boldsymbol{B}_d(\boldsymbol{C}_d\boldsymbol{B}_d)^{-1} \\ \hline -(\boldsymbol{C}_d\boldsymbol{B}_d)^{-1}\boldsymbol{C}_d\boldsymbol{A}_d & (\boldsymbol{C}_d\boldsymbol{B}_d)^{-1} \end{array}\right]. \tag{12}$$

When $\tilde{\boldsymbol{G}}_d^{-1}$ has unstable poles, it can be decomposed as

$$\begin{bmatrix} \boldsymbol{x}_s[k+1] \\ \boldsymbol{x}_u[k+1] \end{bmatrix} = \begin{bmatrix} \boldsymbol{A}_s & \boldsymbol{O} \\ \boldsymbol{O} & \boldsymbol{A}_u \end{bmatrix} \begin{bmatrix} \boldsymbol{x}_s[k] \\ \boldsymbol{x}_u[k] \end{bmatrix} + \begin{bmatrix} \boldsymbol{B}_s \\ \boldsymbol{B}_u \end{bmatrix} \boldsymbol{r}[k+1], \tag{13}$$

$$\boldsymbol{u}[k] = \begin{bmatrix} \boldsymbol{C}_s & \boldsymbol{C}_u \end{bmatrix} \begin{bmatrix} \boldsymbol{x}_s[k] \\ \boldsymbol{x}_u[k] \end{bmatrix} + \boldsymbol{D}\boldsymbol{r}[k+1], \tag{14}$$

where $|\lambda(\boldsymbol{A}_s)| \le 1$ and $|\lambda(\boldsymbol{A}_u)| > 1$. The bounded feedforward input u is given by

$$\boldsymbol{u}[k] = \boldsymbol{C}_s \boldsymbol{x}_s[k] + \boldsymbol{C}_u \boldsymbol{x}_u[k] + \boldsymbol{D}\boldsymbol{r}[k+1] \tag{15}$$

where $\boldsymbol{x}_s$ follows from solving

$$\boldsymbol{x}_s[k+1] = \boldsymbol{A}_s \boldsymbol{x}_s[k] + \boldsymbol{B}_s \boldsymbol{r}[k+1],\ \boldsymbol{x}_s[-\infty] = \boldsymbol{0} \tag{16}$$

forward in time and $\boldsymbol{x}_u$ follows from solving

$$\boldsymbol{x}_u[k+1] = \boldsymbol{A}_u \boldsymbol{x}_u[k] + \boldsymbol{B}_u \boldsymbol{r}[k+1],\ \boldsymbol{x}_u[\infty] = \boldsymbol{0} \tag{17}$$

backward in time (van Zundert & Oomen, 2018). This stable inversion approach is based on that the unstable poles $|\lambda(\boldsymbol{A}_u)| > 1$ forward in time are stable poles $|\lambda(\boldsymbol{A}_u)^{-1}| < 1$ backward in time. The generated feedforward input u provides perfect output tracking for every sample.

Note that although the feedforward input generated by the single-rate stable inversion approach is bounded, the oscillating poles around $\lambda = -1$ cannot be compensated. The oscillating feedforward input can deteriorate intersample performance. The single-rate feedforward controller has unstable or oscillating poles when the relative degree of the continuous-time model is 2 or more as Euler–Frobenius polynomials (Åström et al., 1984).

2.3. Multirate feedforward control for full-state tracking

To compensate for oscillating poles of the feedforward controller due to discretization, multirate feedforward control (Fujimoto et al., 2001) based on perfect state tracking is presented.

The n samples lifted system $\underline{\boldsymbol{H}}_d$ of $\boldsymbol{H}_d \overset{z}{=} (\boldsymbol{A}_d, \boldsymbol{B}_d, \boldsymbol{C}_d, \boldsymbol{D}_d)$ is generally defined as

$$\underline{\boldsymbol{H}}_d \overset{z^n}{=} \mathcal{L}_n \boldsymbol{H}_d \mathcal{L}_n^{-1} = \left[\begin{array}{c|c} \underline{\boldsymbol{A}}_d & \underline{\boldsymbol{B}}_d \\ \hline \underline{\boldsymbol{C}}_d & \underline{\boldsymbol{D}}_d \end{array}\right]$$

$$= \left[\begin{array}{c|ccccc} \boldsymbol{A}_d^n & \boldsymbol{A}_d^{n-1}\boldsymbol{B}_d & \boldsymbol{A}_d^{n-2}\boldsymbol{B}_d & \cdots & \boldsymbol{A}_d\boldsymbol{B}_d & \boldsymbol{B}_d \\ \hline \boldsymbol{C}_d & \boldsymbol{D}_d & \boldsymbol{O} & \cdots & \cdots & \boldsymbol{O} \\ \boldsymbol{C}_d\boldsymbol{A}_d & \boldsymbol{C}_d\boldsymbol{B}_d & \boldsymbol{D}_d & \ddots & & \vdots \\ \vdots & \vdots & \ddots & \ddots & \ddots & \vdots \\ \boldsymbol{C}_d\boldsymbol{A}_d^{n-2} & \boldsymbol{C}_d\boldsymbol{A}_d^{n-3}\boldsymbol{B}_d & \boldsymbol{C}_d\boldsymbol{A}_d^{n-4}\boldsymbol{B}_d & \ddots & \boldsymbol{D}_d & \boldsymbol{O} \\ \boldsymbol{C}_d\boldsymbol{A}_d^{n-1} & \boldsymbol{C}_d\boldsymbol{A}_d^{n-2}\boldsymbol{B}_d & \boldsymbol{C}_d\boldsymbol{A}_d^{n-3}\boldsymbol{B}_d & \cdots & \boldsymbol{C}_d\boldsymbol{B}_d & \boldsymbol{D}_d \end{array}\right] \tag{18}$$

$$\underline{\boldsymbol{u}}[i_n] = \mathcal{L}_n \boldsymbol{u}[k] = \left[\boldsymbol{u}[ni_n] \quad \cdots \quad \boldsymbol{u}[ni_n + (n-1)]\right]^\mathsf{T}$$

$$= \left[u_1[ni_n] \quad \cdots \quad u_m[ni_n] \quad \cdots \quad u_m[ni_n + (n-1)]\right]^\mathsf{T} \in \mathbb{R}^{(m\times n)}, \tag{19}$$

$$\underline{\boldsymbol{y}}[i_n] = \mathcal{L}_n \boldsymbol{y}[k] = \left[\boldsymbol{y}[ni_n] \quad \cdots \quad \boldsymbol{y}[ni_n + (n-1)]\right]^\mathsf{T}$$

$$= \left[y_1[ni_n] \quad \cdots \quad y_m[ni_n] \quad \cdots \quad y_m[ni_n + (n-1)]\right]^\mathsf{T} \in \mathbb{R}^{(m\times n)}, \tag{20}$$

where $\underline{\boldsymbol{u}}[i_n]$ and $\underline{\boldsymbol{y}}[i_n]$ are column vectors, and $\mathcal{L}_n$ is n samples lifting operator (Chen & Francis, 1995).

The N ($\leq n$) samples lifted system of $\boldsymbol{G}_d$ is given by

$$\underline{\boldsymbol{G}}_d \overset{z^N}{=} \mathcal{L}_N \boldsymbol{G}_d \mathcal{L}_N^{-1} = \left[\begin{array}{c|c} \underline{\boldsymbol{A}}_d & \underline{\boldsymbol{B}}_d \\ \hline \underline{\boldsymbol{C}}_d & \underline{\boldsymbol{D}}_d \end{array}\right]. \tag{21}$$

Note that the number of lifting samples is $N = n$ in SISO systems but it is not the case in MIMO systems, see Mae, Ohnishi, and Fujimoto (2020). The desired state trajectory of $\underline{\boldsymbol{G}}_d$ is given by the multirate sampler for every N sample S_N that is defined as

$$\hat{\boldsymbol{x}}[i_N] = S_N \hat{\boldsymbol{x}}(t) = \hat{\boldsymbol{x}}(i_N N\delta), \tag{22}$$

where $\hat{\boldsymbol{x}}(t)$ is the desired state trajectory in continuous time. By inverting the state equation of $\underline{\boldsymbol{G}}_d$, the input u generated by the multirate feedforward controller is given by

$$\begin{aligned}\boldsymbol{u}[k] &= \mathcal{L}_N^{-1}\left(\underline{\boldsymbol{B}}_d^{-1}\hat{\boldsymbol{x}}[i_N+1] - \underline{\boldsymbol{B}}_d^{-1}\underline{\boldsymbol{A}}_d\hat{\boldsymbol{x}}[i_N]\right) \\ &= \mathcal{L}_N^{-1}\underline{\boldsymbol{B}}_d^{-1}(\boldsymbol{I} - z^{-N}\underline{\boldsymbol{A}}_d)\hat{\boldsymbol{x}}[i_N+1],\end{aligned} \tag{23}$$

where z is shift operator in sampling time δ. The generated feedforward input $\boldsymbol{u}$ provides perfect state tracking for every N sample and improves intersample performance.

Note that the desired state trajectory $\hat{\boldsymbol{x}}$ is given by the reference and its derivatives in continuous time for the model without zeros in controllable canonical form. When the model has zeros, the desired state trajectory generation method that is described in the next section is used. Although the multirate feedforward controller provides perfect state tracking for every N sample, the sampling time of the desired state trajectory is $N\delta$, and the higher N is, the lower the reference sampling frequency $1/N\delta$ is.

2.4. Problem description

From these discussions, the optimal perfect tracking controller should be designed by considering the following requirements.

Requirement 1. *Oscillating poles of the feedforward controller due to discretization is compensated by state tracking.*

Requirement 2. *States for perfect tracking control are selected to make reference sampling frequency enough high.*

The state tracking can be provided by multirate feedforward control and the states can be selected based on the mode decomposition. In this paper, two kinds of multirate feedforward controllers with mode selection in additive decomposition (Mae et al., 2021; Ohnishi & Fujimoto, 2018) and multiplicative decomposition (van Zundert et al., 2020) are described and intersample performance is compared with pre-existing perfect tracking control approaches.

In this paper, square systems that have the same number of inputs and outputs are assumed. For applications in industrial mechatronic systems, it is usual to design a static decoupling controller by coordinate transformation and make the controlled system square and statically decoupled in the rigid-body mode. The over-actuated non-square systems are not assumed in this paper because the exact and causal inversion can be achieved by the dynamic squaring-down approach (van Zundert, Luijten, & Oomen, 2019).

Note that the controller design is addressed in both continuous and discrete time to deal with the sampled-data system. Basically, the desired state trajectory generation is conducted in continuous time and the multirate feedforward controller design is conducted in discrete time.

3. Desired state trajectory generation

In this section, the desired state trajectory methods are presented for the SISO and MIMO systems. For the SISO system, the desired state trajectory is generated in controllable canonical form. For the MIMO system, the desired state trajectory is generated by the state transformation using the singular value decomposition of the input matrix. The bounded desired state trajectory is generated by the stable and unstable decomposition and the non-causal convolution with time axis reversal. This paper substantially extends the preliminary result in Mae, Ohnishi, and Fujimoto (2019), Ohnishi et al. (2019) with generalization and theoretical proof in MIMO systems.

3.1. Desired state trajectory generation for SISO system

The single-input single-output continuous-time linear time-invariant n^{th} order system is given by

$$G_c(s) = \frac{B(s)}{A(s)} = \frac{b_m s^m + \cdots + b_1 s + b_0}{s^n + a_{n-1}s^{n-1} + \cdots + a_1 s + a_0}, \tag{24}$$

where $n > m$ and $b_0 \neq 0$. G_c in controllable canonical form $G_{c,ccf} \overset{s}{=} (\boldsymbol{A}_{c,ccf}, \boldsymbol{b}_{c,ccf}, \boldsymbol{c}_{c,ccf}, 0)$ is given by

$$\dot{\boldsymbol{x}}_{ccf}(t) = \boldsymbol{A}_{c,ccf}\boldsymbol{x}_{ccf}(t) + \boldsymbol{b}_{c,ccf}u(t), \tag{25}$$

$$y(t) = \boldsymbol{c}_{c,ccf}\boldsymbol{x}_{ccf}(t), \tag{26}$$

where

$$\left[\begin{array}{c|c} \boldsymbol{A}_{c,ccf} & \boldsymbol{b}_{c,ccf} \\ \hline \boldsymbol{c}_{c,ccf} & 0 \end{array}\right] = \left[\begin{array}{ccccc|c} 0 & 1 & & 0 & 0 \\ & \ddots & \ddots & & \vdots \\ 0 & & 0 & 1 & 0 \\ -a_0 & \cdots & \cdots & -a_{n-1} & 1 \\ \hline b_0 & \cdots & b_m & 0 & 0 \end{array}\right]. \tag{27}$$

The filter for the state trajectory generation is given by

$$\beta(t) = \mathcal{L}^{-1}\left[B(s)^{-1}\right], \tag{28}$$

where $\mathcal{L}[\cdot]$ is the unilateral Laplace transform. The desired state trajectory in the controllable canonical form is given by

$$\hat{\boldsymbol{x}}_{ccf}(t) = \int_0^t \beta(t-\tau)\bar{\boldsymbol{r}}_n(\tau)\mathrm{d}\tau, \tag{29}$$

where

$$\hat{\boldsymbol{x}}_{ccf}(t) = \left[\hat{x}_{ccf,0}(t) \quad \cdots \quad \hat{x}_{ccf,n-1}(t)\right]^\mathsf{T}, \tag{30}$$

$$\bar{\boldsymbol{r}}_n(t) = \left[1 \quad \cdots \quad \frac{\mathrm{d}^{n-1}}{\mathrm{d}t^{n-1}}\right]^\mathsf{T} r(t). \tag{31}$$

When $B(s)^{-1}$ has unstable poles, it can be decomposed as

$$B(s)^{-1} = B_s^{-1}(s) + B_u^{-1}(s), \tag{32}$$

where all poles $p_s \in \mathbb{C}$ of $B_s^{-1}(s)$ are $\mathrm{Re}(p_s) \le 0$ and all poles $p_u \in \mathbb{C}$ of $B_u^{-1}(s)$ are $\mathrm{Re}(p_u) > 0$. The filters of stable and unstable parts for the state trajectory generation are given by

$$\beta_s(t) = \mathcal{L}^{-1}\left[B_s^{-1}(s)\right], \tag{33}$$

$$\beta_u(t) = \mathcal{L}^{-1}\left[B_u^{-1}(-s)\right]. \tag{34}$$

The stable and unstable parts of the desired state trajectory are given by

$$\hat{\boldsymbol{x}}_s(t) = \int_{-\infty}^{t} \beta_s(t-\tau)\bar{r}_n(\tau)\mathrm{d}\tau, \tag{35}$$

$$\hat{\boldsymbol{x}}_u(t) = \int_{t}^{\infty} \beta_u(t-\tau)\bar{r}_n(\tau)\mathrm{d}\tau, \tag{36}$$

and the bounded desired state trajectory in controllable canonical form $\hat{\boldsymbol{x}}_{ccf}$ is given by

$$\hat{\boldsymbol{x}}_{ccf}(t) = \hat{\boldsymbol{x}}_s(t) + \hat{\boldsymbol{x}}_u(t). \tag{37}$$

The state transformation of the system $\boldsymbol{H} = (\boldsymbol{A}, \boldsymbol{B}, \boldsymbol{C}, \boldsymbol{D})$ with the state transformation matrix $\boldsymbol{T}$ is generally defined as

$$\mathcal{T}(\boldsymbol{H}, \boldsymbol{T}) = \left[\begin{array}{c|c} \boldsymbol{T}\boldsymbol{A}\boldsymbol{T}^{-1} & \boldsymbol{T}\boldsymbol{B} \\ \hline \boldsymbol{C}\boldsymbol{T}^{-1} & \boldsymbol{D} \end{array}\right]. \tag{38}$$

The state transformation matrix $\boldsymbol{T}_{ccf}^{-1}$ from the system in controllable canonical form G_{ccf} to the system $G_c \overset{s}{=} (\boldsymbol{A}_c, \boldsymbol{b}_c, \boldsymbol{c}_c, 0)$ with the states $\boldsymbol{x}$ is given by

$$\boldsymbol{T}_{ccf}^{-1} = \begin{bmatrix} \boldsymbol{B}_c & \cdots & \boldsymbol{A}_c^{n-1}\boldsymbol{B}_c \end{bmatrix} \begin{bmatrix} a_1 & \cdots & a_{n-1} & 1 \\ \vdots & \iddots & \iddots & \\ a_{n-1} & \iddots & & \\ 1 & & & \boldsymbol{O} \end{bmatrix}, \tag{39}$$

where

$$G_{c,ccf} = \mathcal{T}(G_c, \boldsymbol{T}_{ccf}), \tag{40}$$

$$\boldsymbol{x}_{ccf}(t) = \boldsymbol{T}_{ccf}\boldsymbol{x}(t). \tag{41}$$

3.2. Desired state trajectory generation for MIMO system

The m-input m-output n^{th} order continuous-time linear time-invariant system $\boldsymbol{G}_c \overset{s}{=} (\boldsymbol{A}_c, \boldsymbol{B}_c, \boldsymbol{C}_c, \boldsymbol{O})$ is given by

$$\dot{\boldsymbol{x}}(t) = \boldsymbol{A}_c\boldsymbol{x}(t) + \boldsymbol{B}_c\boldsymbol{u}(t), \tag{42}$$

$$\boldsymbol{y}(t) = \boldsymbol{C}_c\boldsymbol{x}(t), \tag{43}$$

where $\boldsymbol{A}_c \in \mathbb{R}^{n\times n}$, $\boldsymbol{B}_c \in \mathbb{R}^{n\times m}$, and $\boldsymbol{C}_c \in \mathbb{R}^{m\times n}$. Singular Value Decomposition (SVD) of $\boldsymbol{B}_c$ is given by

$$\boldsymbol{B}_c = \boldsymbol{U}\boldsymbol{\Sigma}\boldsymbol{V}^{\mathsf{H}}, \tag{44}$$

where $\boldsymbol{U} \in \mathbb{R}^{n\times n}$ and $\boldsymbol{V} \in \mathbb{R}^{m\times m}$ are unitary matrices so that $\boldsymbol{U}^{-1} = \boldsymbol{U}^{\mathsf{H}}$ and $\boldsymbol{V}^{-1} = \boldsymbol{V}^{\mathsf{H}}$. The elements of $\boldsymbol{\Sigma} \in \mathbb{R}^{n\times m}$ are given by

$$\boldsymbol{\Sigma} = \begin{bmatrix} \boldsymbol{\Delta} \\ \boldsymbol{O} \end{bmatrix}, \tag{45}$$

$$\boldsymbol{\Delta} = \mathrm{diag}(\sigma_i) \quad (i = 1 \cdots m \in \mathbb{N}), \tag{46}$$

where σ_i $(i = 1 \cdots m \in \mathbb{N})$ are the singular values of $\boldsymbol{B}$.

The system $\boldsymbol{G}_{svd} \overset{s}{=} (\boldsymbol{A}_{svd}, \boldsymbol{B}_{svd}, \boldsymbol{C}_{svd}, \boldsymbol{O}) = \mathcal{T}(\boldsymbol{G}_c, \boldsymbol{U}^{\mathsf{H}})$ with the states $\boldsymbol{x}_{svd} = \boldsymbol{U}^{\mathsf{H}}\boldsymbol{x}$ is given by

$$\left[\begin{array}{c|c} \boldsymbol{W}_u(s) & \boldsymbol{\Delta}\boldsymbol{V}^{\mathsf{H}} \\ \hline \boldsymbol{W}_l(s) & \boldsymbol{O}_{(n-m)\times m} \\ \boldsymbol{C}_{svd} & \boldsymbol{O}_{m\times m} \end{array}\right] \left[\begin{array}{c} \boldsymbol{x}_{svd}(s) \\ \hline \boldsymbol{u}(s) \end{array}\right] = \left[\begin{array}{c} \boldsymbol{O}_{m\times m} \\ \hline \boldsymbol{O}_{(n-m)\times m} \\ \boldsymbol{y}(s) \end{array}\right], \tag{47}$$

where $\boldsymbol{u}(s) = \mathcal{L}[\boldsymbol{u}(t)]$, $\boldsymbol{x}(s) = \mathcal{L}[\boldsymbol{x}(t)]$, $\boldsymbol{y}(s) = \mathcal{L}[\boldsymbol{y}(t)]$, $\boldsymbol{W}_u(s) \in \mathbb{R}^{m\times n}$, $\boldsymbol{W}_l(s) \in \mathbb{R}^{(n-m)\times n}$, and the Rosenbrock system matrix $\boldsymbol{\Pi}_{svd}(s)$ is given by

$$\boldsymbol{\Pi}_{svd}(s) = \left[\begin{array}{c|c} \boldsymbol{A}_{svd} - s\boldsymbol{I} & \boldsymbol{B}_{svd} \\ \hline \boldsymbol{C}_{svd} & \boldsymbol{O} \end{array}\right] = \left[\begin{array}{c|c} \boldsymbol{W}_u(s) & \boldsymbol{\Delta}\boldsymbol{V}^{\mathsf{H}} \\ \hline \boldsymbol{W}_l(s) & \boldsymbol{O}_{(n-m)\times m} \\ \boldsymbol{C}_{svd} & \boldsymbol{O}_{m\times m} \end{array}\right]. \tag{48}$$

The following theorem shows that $\boldsymbol{W}_l(s)$ contains the property for the invariant zeros of the system.

Theorem 1 (*Identity of Invariant Zeros*)**.** *Invariant zeros of $\boldsymbol{G}_{svd}$ are the values when $\boldsymbol{W}_l(s)$ is not full row rank.*

Proof. The invariant zero is defined as the value when the Rosenbrock system matrix is not full rank. It is assumed that $\mathrm{rank}(\boldsymbol{\Delta}\boldsymbol{V}^{\mathsf{H}}) = m$ and the upper m rows of $\boldsymbol{\Pi}_{svd}(s)$ are full row rank. It is assumed that $\mathrm{rank}(\boldsymbol{C}_c) = m$ and $\mathrm{rank}(\boldsymbol{U}) = n$. From Sylvester's rank inequality, for $\boldsymbol{X} \in \mathbb{R}^{l\times n}$ and $\boldsymbol{X} \in \mathbb{R}^{n\times k}$ it generally follows

$$\mathrm{rank}(\boldsymbol{X}) + \mathrm{rank}(\boldsymbol{Y}) - n \le \mathrm{rank}(\boldsymbol{X}\boldsymbol{Y}). \tag{49}$$

Sylvester's rank inequality is applied to $\boldsymbol{X}$ as $\boldsymbol{C}_c$ and $\boldsymbol{Y}$ as $\boldsymbol{U}$. It follows that $\mathrm{rank}(\boldsymbol{C}_{svd}) = \mathrm{rank}(\boldsymbol{C}_c\boldsymbol{U}) = m$ and the lower m rows of $\boldsymbol{\Pi}_{svd}(s)$ are full row rank. Therefore, the values when $\boldsymbol{W}_l(s)$ is not full rank are the same as the values when the Rosenbrock system matrix is not full rank. □

From (47),

$$\left[\begin{array}{c} \boldsymbol{W}_l(s) \\ \hline \boldsymbol{C}_{svd} \end{array}\right] \boldsymbol{x}_{svd}(s) = \left[\begin{array}{c} \boldsymbol{O}_{(n-m)\times m} \\ \hline \boldsymbol{y}(s) \end{array}\right], \tag{50}$$

and it follows that

$$\boldsymbol{x}_{svd}(s) = \left[\begin{array}{c} \boldsymbol{W}_l(s) \\ \hline \boldsymbol{C}_{svd} \end{array}\right]^{-1} \left[\begin{array}{c} \boldsymbol{O}_{(n-m)\times m} \\ \hline \boldsymbol{y}(s) \end{array}\right]. \tag{51}$$

Let the state transformation be

$$\boldsymbol{x}(s) = \boldsymbol{U}\boldsymbol{x}_{svd}(s) = \boldsymbol{U}\left[\begin{array}{c} \boldsymbol{W}_l(s) \\ \hline \boldsymbol{C}_{svd} \end{array}\right]^{-1} \left[\begin{array}{c} \boldsymbol{O}_{(n-m)\times m} \\ \hline \boldsymbol{y}(s) \end{array}\right]. \tag{52}$$

Let the inverse Laplace transform be $\boldsymbol{\beta}(t) = \mathcal{L}^{-1}[\boldsymbol{B}^{-1}(s)]$, where

$$\boldsymbol{B}^{-1}(s) = \boldsymbol{U}\left[\begin{array}{c} \boldsymbol{W}_l(s) \\ \hline \boldsymbol{C}_{svd} \end{array}\right]^{-1}. \tag{53}$$

The desired state trajectory is given by

$$\hat{\boldsymbol{x}}(t) = \int_0^t \boldsymbol{\beta}(t-\tau)\begin{bmatrix} \boldsymbol{O}_{(n-m)\times m} \\ \boldsymbol{r}(\tau) \end{bmatrix}\mathrm{d}\tau. \tag{54}$$

When $\boldsymbol{B}(s)^{-1}$ has unstable poles, it can be decomposed as

$$\boldsymbol{B}(s)^{-1} = \boldsymbol{B}_s^{-1}(s) + \boldsymbol{B}_u^{-1}(s), \tag{55}$$

where all poles $p_s \in \mathbb{C}$ of $\boldsymbol{B}_s^{-1}(s)$ are $\mathrm{Re}(p_s) \le 0$ and all poles $p_u \in \mathbb{C}$ of $\boldsymbol{B}_u^{-1}(s)$ are $\mathrm{Re}(p_u) > 0$. The filter matrices of stable and unstable parts for the state trajectory generation are given by

$$\boldsymbol{\beta}_s(t) = \mathcal{L}^{-1}\left[\boldsymbol{B}_s^{-1}(s)\right], \tag{56}$$

$$\boldsymbol{\beta}_u(t) = \mathcal{L}^{-1}\left[\boldsymbol{B}_u^{-1}(-s)\right]. \tag{57}$$

The stable and unstable parts of the desired state trajectory are given by

$$\hat{\boldsymbol{x}}_s(t) = \int_{-\infty}^{t} \boldsymbol{\beta}_s(t-\tau)\begin{bmatrix} \boldsymbol{O}_{(n-m)\times m} \\ \boldsymbol{r}(\tau) \end{bmatrix}\mathrm{d}\tau, \tag{58}$$

$$\hat{\boldsymbol{x}}_u(t) = \int_{t}^{\infty} \boldsymbol{\beta}_u(t-\tau)\begin{bmatrix} \boldsymbol{O}_{(n-m)\times m} \\ \boldsymbol{r}(\tau) \end{bmatrix}\mathrm{d}\tau, \tag{59}$$

and the bounded desired state trajectory $\hat{\boldsymbol{x}}$ is given by

$$\hat{\boldsymbol{x}}(t) = \hat{\boldsymbol{x}}_s(t) + \hat{\boldsymbol{x}}_u(t). \tag{60}$$

Note that the unitary matrix $\boldsymbol{U}$ that is used as the state transformation matrix is not unique in singular value decomposition but the desired state trajectory is generated uniquely for the desired state-space representation. The calculation of the singular value decomposition can be numerically ill-conditioned and the state-space representation should be properly formulated so that the state transformation matrix $\boldsymbol{U}$ is not numerically ill-conditioned.

4. Multirate feedforward control with mode decomposition

In this section, the multirate feedforward control with mode decomposition is presented. First, the model of the multi-modal motion system is defined. Second, the multirate feedforward control with additive decomposition is described. Third, the multirate feedforward control with multiplicative decomposition is described. The intersample performance of these two approaches is verified in the next section.

4.1. Definition of multi-modal motion system

The m-input m-output continuous-time multi-modal motion system (Gawronski, 2004) is defined as

$$\boldsymbol{G}_c(s) = \sum_{k_m=1}^{n_m} \frac{\boldsymbol{c}_{k_m}\boldsymbol{b}_{k_m}}{s^2 + 2\zeta_{k_m}\omega_{k_m}s + \omega_{k_m}^2} = \sum_{k_m=1}^{n_m} \boldsymbol{G}_{c,mod,k_m}(s), \tag{61}$$

where ω is the resonance angle frequency, ζ is the damping coefficient, and n_m is the number of modes. The vectors $\boldsymbol{b} \in \mathbb{R}^{1\times m}$ and $\boldsymbol{c} \in \mathbb{R}^{m\times 1}$ are associated with the inputs, the outputs, and the mode shapes. $\boldsymbol{G}_c$ in modal form $\boldsymbol{G}_{c,mod} \overset{s}{=} (\boldsymbol{A}_{c,mod}, \boldsymbol{B}_{c,mod}, \boldsymbol{C}_{c,mod}, \boldsymbol{O})$ is given by

$$\dot{\boldsymbol{x}}_{mod}(t) = \boldsymbol{A}_{c,mod}\boldsymbol{x}_{mod}(t) + \boldsymbol{B}_{c,mod}\boldsymbol{u}(t), \tag{62}$$

$$\boldsymbol{y}(t) = \boldsymbol{C}_{c,mod}\boldsymbol{x}_{mod}(t), \tag{63}$$

where

$$\left[\begin{array}{c|c} \boldsymbol{A}_{c,mod} & \boldsymbol{B}_{c,mod} \\ \hline \boldsymbol{C}_{c,mod} & \boldsymbol{O} \end{array}\right] = \left[\begin{array}{ccc|c} \boldsymbol{A}_{c,mod,1} & & \boldsymbol{O} & \boldsymbol{B}_{c,mod,1} \\ & \ddots & & \vdots \\ \boldsymbol{O} & & \boldsymbol{A}_{c,mod,n_m} & \boldsymbol{B}_{c,mod,n_m} \\ \hline \boldsymbol{C}_{c,mod,1} & \cdots & \boldsymbol{C}_{c,mod,n_m} & \boldsymbol{O} \end{array}\right], \tag{64}$$

$$\boldsymbol{x}_{mod}(t) = \begin{bmatrix} \boldsymbol{x}_{mod,1}(t) & \cdots & \boldsymbol{x}_{mod,n_m}(t) \end{bmatrix}^\mathsf{T}, \tag{65}$$

and the subsystem $\boldsymbol{G}_{c,mod,k_m} \overset{s}{=} (\boldsymbol{A}_{c,mod,k_m}, \boldsymbol{B}_{c,mod,k_m}, \boldsymbol{C}_{c,mod,k_m}, \boldsymbol{O})$ is given by

$$\left[\begin{array}{c|c} \boldsymbol{A}_{c,mod,k_m} & \boldsymbol{B}_{c,mod,k_m} \\ \hline \boldsymbol{C}_{c,mod,k_m} & \boldsymbol{O} \end{array}\right] = \left[\begin{array}{cc|c} 0 & 1 & \boldsymbol{O} \\ -\omega_{k_m}^2 & -2\zeta_{k_m}\omega_{k_m} & \boldsymbol{b}_{k_m} \\ \hline \boldsymbol{c}_{k_m} & \boldsymbol{O} & \boldsymbol{O} \end{array}\right]. \tag{66}$$

$$\boldsymbol{x}_{mod,k_m}(t) = \begin{bmatrix} x_{mod,k_m,0}(t) & x_{mod,k_m,1}(t) \end{bmatrix}^\mathsf{T}. \tag{67}$$

Although there are other representations such as the numerical decomposed model, the multi-modal model is reasonable for the intersample performance improvement by the state tracking control, and mode selection should be relied on the physical meaning of the states. The state tracking is only guaranteed on-sample and the intersample performance improvement is achieved because of the physical relationships between each state. The gray box modeling approach with white box structure and black box parameter tuning such as in Voorhoeve, de Rozario, Aangenent, and Oomen (2021) is preferable to obtain the high-order multi-modal model in which each mode has a physical interpretation of the mode shapes.

4.2. Multirate feedforward control with additive decomposition

The overview of multirate feedforward control with additive decomposition (Mae et al., 2021; Ohnishi & Fujimoto, 2018) is shown in Fig. 2. The indices μ of the selected modes are defined as

$$\mu = \{k_m | k_m \in 1, \dots, n_m\}, \tag{68}$$

and the order ν of the selected modes is defined as

$$\nu = 2 \times \text{number}\{\mu\}. \tag{69}$$

The permutation matrix for the selected modes is defined as

$$\boldsymbol{T}_\mu = \begin{bmatrix} \boldsymbol{E}_\mu \\ \boldsymbol{E}_\times \end{bmatrix}, \tag{70}$$

where $\boldsymbol{E}_\mu$ and $\boldsymbol{E}_\times$ consist of standard basis vectors of selected and unselected modes, and the standard basis vectors of the mode k_m is defined as

$$\boldsymbol{E}_{k_m} = \begin{bmatrix} \boldsymbol{O}_{2\times 2(k_m-1)} & \boldsymbol{I}_2 & \boldsymbol{O}_{2\times 2(n_m-k_m)} \end{bmatrix}. \tag{71}$$

The model reduction matrix extracting upper ν states is defined as

$$\boldsymbol{T}_\nu = \begin{bmatrix} \boldsymbol{I}_\nu & \boldsymbol{O}_{\nu\times(n-\nu)} \end{bmatrix}. \tag{72}$$

The system of the selected modes $\boldsymbol{G}_{c,\mu}$ is given by

$$\dot{\boldsymbol{x}}_\mu(t) = \boldsymbol{A}_{c,\mu}\boldsymbol{x}_\mu(t) + \boldsymbol{B}_{c,\mu}\boldsymbol{u}(t), \tag{73}$$

$$\boldsymbol{y}(t) = \boldsymbol{C}_{c,\mu}\boldsymbol{x}_\mu(t), \tag{74}$$

where

$$\boldsymbol{x}_\mu(t) = \boldsymbol{T}_\nu\boldsymbol{T}_\mu\boldsymbol{x}_{mod}(t), \tag{75}$$

$$\boldsymbol{A}_{c,\mu} = \boldsymbol{T}_\nu\boldsymbol{T}_\mu\boldsymbol{A}_{c,mod}\boldsymbol{T}_\mu^{-1}\boldsymbol{T}_\nu^\mathsf{T}, \tag{76}$$

$$\boldsymbol{B}_{c,\mu} = \boldsymbol{T}_\nu\boldsymbol{T}_\mu\boldsymbol{B}_{c,mod}, \tag{77}$$

$$\boldsymbol{C}_{c,\mu} = \boldsymbol{C}_{c,mod}\boldsymbol{T}_\mu^{-1}\boldsymbol{T}_\nu^\mathsf{T}. \tag{78}$$

The discrete-time system of $\boldsymbol{G}_{c,\mu}$ is given by

$$\boldsymbol{G}_{d,\mu} \overset{z}{=} S\boldsymbol{G}_{c,\mu}\mathcal{H} = \left[\begin{array}{c|c} \boldsymbol{A}_{d,\mu} & \boldsymbol{B}_{d,\mu} \\ \hline \boldsymbol{C}_{d,\mu} & \boldsymbol{O} \end{array}\right], \tag{79}$$

and the N ($\leq \nu$) samples lifted system of $\boldsymbol{G}_{d,\mu}$ is given by

$$\underline{\boldsymbol{G}}_{d,\mu} \overset{z^N}{=} \mathcal{L}_N\boldsymbol{G}_{d,\mu}\mathcal{L}_N^{-1} = \left[\begin{array}{c|c} \underline{\boldsymbol{A}}_{d,\mu} & \underline{\boldsymbol{B}}_{d,\mu} \\ \hline \underline{\boldsymbol{C}}_{d,\mu} & \underline{\boldsymbol{D}}_{d,\mu} \end{array}\right]. \tag{80}$$

Note that the number of lifting samples is $N = \nu$ in SISO systems but it is not the case in MIMO systems, see Mae et al. (2020). By inverting the state equation of $\underline{\boldsymbol{G}}_{d,\mu}$, the input $\boldsymbol{u}$ generated by the multirate feedforward controller with additive decomposition is given by

$$\begin{aligned} \boldsymbol{u}[k] &= \mathcal{L}_N^{-1}\left(\underline{\boldsymbol{B}}_{d,\mu}^{-1}\hat{\boldsymbol{x}}_\mu[i_N+1] - \underline{\boldsymbol{B}}_{d,\mu}^{-1}\underline{\boldsymbol{A}}_{d,\mu}\hat{\boldsymbol{x}}_\mu[i_N]\right) \\ &= \mathcal{L}_N^{-1}\underline{\boldsymbol{B}}_{d,\mu}^{-1}(\boldsymbol{I} - z^{-N}\underline{\boldsymbol{A}}_{d,\mu})\hat{\boldsymbol{x}}_\mu[i_N+1], \end{aligned} \tag{81}$$

where $\hat{\boldsymbol{x}}_\mu[i_N] = S_N\boldsymbol{T}_\nu\boldsymbol{T}_\mu\hat{\boldsymbol{x}}_{mod}(t)$. The generated feedforward input $\boldsymbol{u}$ provides perfect state tracking for every N sample for the states corresponding to the selected modes μ.

Note that although perfect state tracking for selected states does not guarantee perfect output tracking, it can provide better intersample performance because the desired state trajectory is generated by the model with full states, and the reference sampling frequency for selected ν states becomes higher to $1/N\delta$ where $N \leq \nu \leq n$.

4.3. Multirate feedforward control with multiplicative decomposition

The overview of multirate feedforward control with multiplicative decomposition (van Zundert et al., 2020) is shown in Fig. 3. The one-sample forward shifted system $\tilde{\boldsymbol{G}}_{d,mod} \overset{z}{=} (\tilde{\boldsymbol{A}}_{d,mod}, \tilde{\boldsymbol{B}}_{d,mod}, \tilde{\boldsymbol{C}}_{d,mod}, \tilde{\boldsymbol{D}}_{d,mod})$ of the discrete-time system in modal form $\boldsymbol{G}_{d,mod} \overset{z}{=} (\boldsymbol{A}_{d,mod}, \boldsymbol{B}_{d,mod}, \boldsymbol{C}_{d,mod}, \boldsymbol{O}) = S\boldsymbol{G}_{c,mod}\mathcal{H}$ from $\boldsymbol{u}[k]$ to $\boldsymbol{y}[k+1]$ is given by

$$\left[\begin{array}{c|c} \tilde{\boldsymbol{A}}_{d,mod} & \tilde{\boldsymbol{B}}_{d,mod} \\ \hline \tilde{\boldsymbol{C}}_{d,mod} & \tilde{\boldsymbol{D}}_{d,mod} \end{array}\right] = \left[\begin{array}{c|c} \boldsymbol{A}_{d,mod} & \boldsymbol{B}_{d,mod} \\ \hline \boldsymbol{C}_{d,mod}\boldsymbol{A}_{d,mod} & \boldsymbol{C}_{d,mod}\boldsymbol{B}_{d,mod} \end{array}\right]. \tag{82}$$

When ν states corresponding to the modes μ are selected,

$$\boldsymbol{\Pi} = \boldsymbol{S}\begin{bmatrix} \boldsymbol{I}_\nu & \boldsymbol{O}_{\nu\times(n-\nu)} \\ \boldsymbol{O}_{(n-\nu)\times\nu} & \boldsymbol{O}_{(n-\nu)} \end{bmatrix}\boldsymbol{S}^{-1} \tag{83}$$

is defined with full rank $\boldsymbol{S} = \begin{bmatrix} \boldsymbol{V} & \boldsymbol{V}_\times \end{bmatrix}$, where $\boldsymbol{V} \in \mathbb{R}^{n\times\nu}$ and $\boldsymbol{V}_\times \in \mathbb{R}^{n\times(n-\nu)}$ are a column space of an invariant subspace of $\boldsymbol{A} = \tilde{\boldsymbol{A}}_{d,mod}$ and $\boldsymbol{A}_\times = \tilde{\boldsymbol{A}}_{d,mod} - \tilde{\boldsymbol{B}}_{d,mod}\tilde{\boldsymbol{D}}_{d,mod}^{-1}\tilde{\boldsymbol{C}}_{d,mod}$ that correspond to the poles of $\boldsymbol{G}_{mr}$ and the zeros of $\boldsymbol{G}_{sr}$. Then the state-space realizations are given by

$$\boldsymbol{G}_{mrf} \overset{z}{=} \left[\begin{array}{c|c} \tilde{\boldsymbol{A}}_{d,mod} & \boldsymbol{\Pi}\tilde{\boldsymbol{B}}_{d,mod}\tilde{\boldsymbol{D}}_{d,mod}^{-1} \\ \hline \tilde{\boldsymbol{C}}_{d,mod} & \boldsymbol{I} \end{array}\right], \tag{84}$$

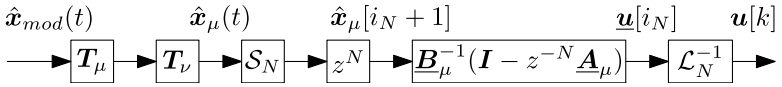

Fig. 2. Block diagram of multirate feedforward control with additive decomposition.

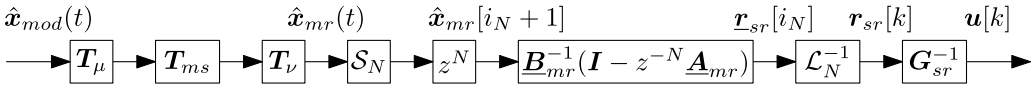

Fig. 3. Block diagram of multirate feedforward control with multiplicative decomposition.

$$\boldsymbol{G}_{srf} \overset{z}{=} \left[\begin{array}{c|c} \tilde{\boldsymbol{A}}_{d,mod} & \tilde{\boldsymbol{B}}_{d,mod} \\ \hline \tilde{\boldsymbol{C}}_{d,mod}(\boldsymbol{I}-\boldsymbol{\Pi}) & \tilde{\boldsymbol{D}}_{d,mod} \end{array}\right]. \tag{85}$$

Let the permutation matrix $\boldsymbol{T}_\mu$ be such that

$$\mathcal{T}(\boldsymbol{G}_{mrf}, \boldsymbol{T}_\mu) \overset{z}{=} \left[\begin{array}{cc|c} \boldsymbol{A}_{mr} & \boldsymbol{O} & \boldsymbol{B}_{mr} \\ \boldsymbol{O} & \boldsymbol{A}_{sr} & \boldsymbol{O} \\ \hline \boldsymbol{C}_{mr} & \boldsymbol{C}_{mrr} & \boldsymbol{I} \end{array}\right], \tag{86}$$

$$\mathcal{T}(\boldsymbol{G}_{srf}, \boldsymbol{T}_\mu) \overset{z}{=} \left[\begin{array}{cc|c} \boldsymbol{A}_{mr} & \boldsymbol{O} & \boldsymbol{B}_{srr} \\ \boldsymbol{O} & \boldsymbol{A}_{sr} & \boldsymbol{B}_{sr} \\ \hline \boldsymbol{O} & \boldsymbol{C}_{sr} & \boldsymbol{D}_{sr} \end{array}\right]. \tag{87}$$

$\boldsymbol{G}_{mr}$ with states $\boldsymbol{x}_{mr}$ and $\boldsymbol{G}_{sr}$ with states $\boldsymbol{x}_{sr}$ are given by

$$\boldsymbol{G}_{mr} \overset{z}{=} \left[\begin{array}{c|c} \boldsymbol{A}_{mr} & \boldsymbol{B}_{mr} \\ \hline \boldsymbol{C}_{mr} & \boldsymbol{I} \end{array}\right], \tag{88}$$

$$\boldsymbol{G}_{sr} \overset{z}{=} \left[\begin{array}{c|c} \boldsymbol{A}_{sr} & \boldsymbol{B}_{sr} \\ \hline \boldsymbol{C}_{sr} & \boldsymbol{D} \end{array}\right]. \tag{89}$$

The product of the system $\boldsymbol{H}_1 = (\boldsymbol{A}_1, \boldsymbol{B}_1, \boldsymbol{C}_1, \boldsymbol{D}_1)$ and $\boldsymbol{H}_2 = (\boldsymbol{A}_2, \boldsymbol{B}_2, \boldsymbol{C}_2, \boldsymbol{D}_2)$ is generally defined as

$$\boldsymbol{H}_1\boldsymbol{H}_2 = \left[\begin{array}{cc|c} \boldsymbol{A}_1 & \boldsymbol{B}_1\boldsymbol{C}_2 & \boldsymbol{B}_1\boldsymbol{D}_2 \\ \boldsymbol{O} & \boldsymbol{A}_2 & \boldsymbol{B}_2 \\ \hline \boldsymbol{C}_1 & \boldsymbol{D}_1\boldsymbol{C}_2 & \boldsymbol{D}_1\boldsymbol{D}_2 \end{array}\right]. \tag{90}$$

The state transformation matrix $\boldsymbol{T}_{ms}$ is given by

$$\boldsymbol{T}_{ms} = \left[\begin{array}{cc} \boldsymbol{I}_\nu & \boldsymbol{X} \\ \boldsymbol{O}_{\nu\times(n-\nu)} & \boldsymbol{I}_{(n-\nu)} \end{array}\right]^{-1}, \tag{91}$$

where $\boldsymbol{X} \in \mathbb{R}^{\nu\times(n-\nu)}$ is the solution of the Sylvester equation

$$\boldsymbol{A}_{mr}\boldsymbol{X} - \boldsymbol{X}\boldsymbol{A}_{sr} = \boldsymbol{B}_{mr}\boldsymbol{C}_{sr}. \tag{92}$$

$\tilde{\boldsymbol{G}}_{ms} \overset{z}{=} (\tilde{\boldsymbol{A}}_{ms}, \tilde{\boldsymbol{B}}_{ms}, \tilde{\boldsymbol{C}}_{ms}, d) = \mathcal{T}(\tilde{\boldsymbol{G}}_{d,mod}, \boldsymbol{T}_{ms}\boldsymbol{T}_\mu) = \boldsymbol{G}_{mr}\boldsymbol{G}_{sr}$ is given by

$$\left[\begin{array}{c|c} \tilde{\boldsymbol{A}}_{ms} & \tilde{\boldsymbol{B}}_{ms} \\ \hline \tilde{\boldsymbol{C}}_{ms} & \boldsymbol{D} \end{array}\right] = \left[\begin{array}{cc|c} \boldsymbol{A}_{mr} & \boldsymbol{B}_{mr}\boldsymbol{C}_{sr} & \boldsymbol{B}_{mr}d \\ \boldsymbol{O} & \boldsymbol{A}_{sr} & \boldsymbol{B}_{sr} \\ \hline \boldsymbol{C}_{mr} & \boldsymbol{C}_{sr} & \boldsymbol{D} \end{array}\right]. \tag{93}$$

The N ($\leq \nu$) samples lifted system of $\boldsymbol{G}_{mr}$ is given by

$$\underline{\boldsymbol{G}}_{mr} \overset{z^N}{=} \mathcal{L}_N\boldsymbol{G}_{mr}\mathcal{L}_N^{-1} = \left[\begin{array}{c|c} \underline{\boldsymbol{A}}_{mr} & \underline{\boldsymbol{B}}_{mr} \\ \hline \underline{\boldsymbol{C}}_{mr} & \boldsymbol{O} \end{array}\right]. \tag{94}$$

Note that the number of lifting samples is $N = \nu$ in SISO systems but it is not the case in MIMO systems, see Mae et al. (2020). By inverting the state equation of $\underline{\boldsymbol{G}}_{mr}$, the reference for the single-rate inversion $\boldsymbol{r}_{sr}$ is given by

$$\begin{aligned} \boldsymbol{r}_{sr}[k] &= \mathcal{L}_N^{-1}\left(\underline{\boldsymbol{B}}_{d,mr}^{-1}\hat{\boldsymbol{x}}_{mr}[i_N+1] - \underline{\boldsymbol{B}}_{d,mr}^{-1}\underline{\boldsymbol{A}}_{d,mr}\hat{\boldsymbol{x}}_{mr}[i_N]\right) \\ &= \mathcal{L}_N^{-1}\underline{\boldsymbol{B}}_{d,mr}^{-1}(\boldsymbol{I}-z^{-N}\underline{\boldsymbol{A}}_{d,mr})\hat{\boldsymbol{x}}_{mr}[i_N+1], \end{aligned} \tag{95}$$

where $\hat{\boldsymbol{x}}_{mr}[i_N] = \mathcal{S}_N\boldsymbol{T}_\nu\boldsymbol{T}_{ms}\boldsymbol{T}_\mu\hat{\boldsymbol{x}}_{mod}(t)$. Then, the input u generated by the multirate feedforward controller with multiplicative decomposition is given by

$$\boldsymbol{u}[k] = \boldsymbol{G}_{sr}^{-1}\boldsymbol{r}_{sr}[k], \tag{96}$$

where

$$\boldsymbol{G}_{sr}^{-1} = \left[\begin{array}{c|c} \boldsymbol{A}_{sr} - \boldsymbol{B}_{sr}\boldsymbol{D}_{sr}^{-1}\boldsymbol{C}_{sr} & \boldsymbol{B}_{sr}\boldsymbol{D}_{sr}^{-1} \\ \hline -\boldsymbol{D}_{sr}^{-1}\boldsymbol{C}_{sr} & \boldsymbol{D}_{sr}^{-1} \end{array}\right]. \tag{97}$$

Note that the one-sample backward shifted system of $\tilde{G}_{ms}$ is given by

$$\begin{aligned} \boldsymbol{G}_{ms} &= \mathcal{T}(\boldsymbol{G}_{d,mod}, \boldsymbol{T}_{ms}\boldsymbol{T}_\mu) = \left[\begin{array}{c|c} \boldsymbol{A}_{ms} & \boldsymbol{B}_{ms} \\ \hline \boldsymbol{C}_{ms} & \boldsymbol{O} \end{array}\right] \\ &= \left[\begin{array}{c|c} \tilde{\boldsymbol{A}}_{ms} & \tilde{\boldsymbol{B}}_{ms} \\ \hline \tilde{\boldsymbol{C}}_{ms}\tilde{\boldsymbol{A}}_{ms}^{-1} & \boldsymbol{O} \end{array}\right] = \left[\begin{array}{cc|c} \boldsymbol{A}_{mr} & \boldsymbol{B}_{mr}\boldsymbol{C}_{sr} & \boldsymbol{B}_{mr}\boldsymbol{D} \\ \boldsymbol{O} & \boldsymbol{A}_{sr} & \boldsymbol{B}_{sr} \\ \hline \boldsymbol{C}_{mr}^* & \boldsymbol{D}_{mr}^*\boldsymbol{C}_{sr}^* & \boldsymbol{D}_{mr}^*\boldsymbol{D} \end{array}\right] \\ &= \left[\begin{array}{c|c} \boldsymbol{A}_{mr} & \boldsymbol{B}_{mr} \\ \hline \boldsymbol{C}_{mr}^* & \boldsymbol{D}_{mr}^* \end{array}\right]\left[\begin{array}{c|c} \boldsymbol{A}_{sr} & \boldsymbol{B}_{sr} \\ \hline \boldsymbol{C}_{sr}^* & \boldsymbol{D} \end{array}\right], \end{aligned} \tag{98}$$

where $\boldsymbol{D}_{mr}^*\boldsymbol{D} = \boldsymbol{O}$ and the output is given by

$$\boldsymbol{y}[k] = \boldsymbol{C}_{mr}^*\boldsymbol{x}_{mr}[k] + \boldsymbol{D}_{mr}^*\boldsymbol{C}_{sr}^*\boldsymbol{x}_{sr}[k]. \tag{99}$$

It shows that the approach provides perfect output tracking for every N sample with $\boldsymbol{D}_{mr}^* = \boldsymbol{O}$ because the multirate inversion provides perfect state tracking of $\boldsymbol{x}_{mr}$ for every N sample. If the system is decomposed as $\boldsymbol{D}_{mr}^* \neq \boldsymbol{O}$, there is no perfect output tracking because perfect state tracking of $\boldsymbol{x}_{sr}$ is not guaranteed. Therefore, $\boldsymbol{V}$ and $\boldsymbol{V}_\times$ should be selected such that $\boldsymbol{D}_{mr}^* = \boldsymbol{O}$.

5. Application to multi-modal motion system

In this section, the intersample performance of the perfect tracking control approaches is validated in a multi-modal motion system. The intersample performance is evaluated in both frequency domain and time domain. The nominal and robust performance is verified in the simulation using the model without and with modeling error. The experimental validation is conducted with feedback controller.

5.1. Conditions

The validation is conducted in a single-input single-output multi-modal motion system in Fig. 4. The frequency response of the controlled system is shown in Fig. 5. For the verification of the modeling error, the high-order continuous-time model $\hat{G}$ is given by

$$\begin{aligned} \hat{G}(s) = {} & \frac{2.44}{s^2} \\ & + \frac{1.1}{s^2 + 2\times0.024\times(2\pi\times30)s + (2\pi\times30)^2} \\ & + \frac{-2.44}{s^2 + 2\times0.038\times(2\pi\times89)s + (2\pi\times89)^2} \\ & + \frac{-1.1}{s^2 + 2\times0.07\times(2\pi\times297)s + (2\pi\times297)^2} \\ = {} & G_1(s) + G_2(s) + G_3(s) + G_4(s). \end{aligned} \tag{100}$$

For the controller design, a low-order continuous-time model G_c is given by

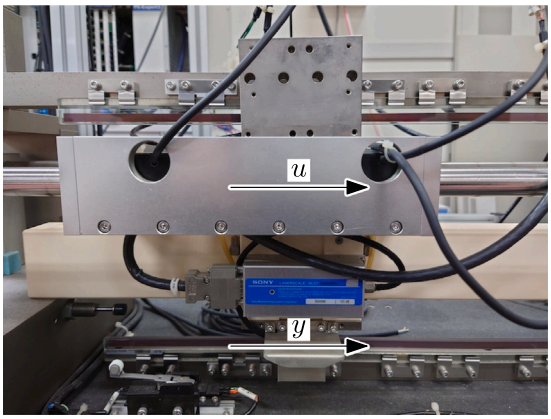

Fig. 4. High-precision positioning stage with input current u [A] generating force with linear motor and output displacement y [m] measured by linear encoder with 1 nm resolution.

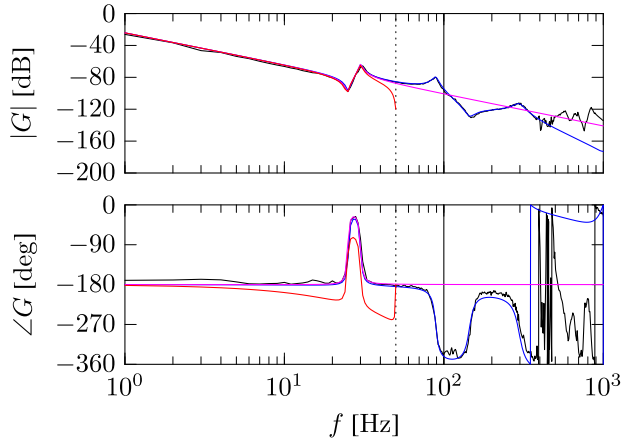

Fig. 5. Bode diagram of the controlled system: frequency response data (——), a high-order continuous-time model $\hat{G}$ (——), a low-order continuous-time model G_c (——), and a low-order discrete-time model for controller design G_d (——). Vertical lines (····) and (——) show Nyquist frequency $1/2\delta$ and sampling frequency $1/\delta$, respectively.

$$
\begin{aligned}
G_c(s) &= G_1(s) + G_2(s) \\
&= \frac{2.44}{s^2} + \frac{1.1}{s^2 + 2 \times 0.024 \times (2\pi \times 30)s + (2\pi \times 30)^2} \\
&= \frac{3.54}{s^2} \times \frac{s^2 + 2 \times 0.02 \times (2\pi \times 25)s + (2\pi \times 25)^2}{s^2 + 2 \times 0.024 \times (2\pi \times 30)s + (2\pi \times 30)^2} \\
&= \frac{N_1(s)}{D_1(s)} \times \frac{N_2(s)}{D_2(s)}.
\end{aligned} \tag{101}
$$

The controller is designed by the low-order continuous-time model G_c and the continuous-time performance is verified by the simulation in the low-order continuous-time model G_c without modeling error and the high-order continuous-time model $\hat{G}$ with modeling error. The verification is conducted in both frequency domain and time domain. The sampling time of the controller is $\delta = 10$ ms. The intersample performance is evaluated in the sampling time $\delta/20 = 0.5$ ms.

The compared 8 approaches are shown in Table 1. The difference in the approach between using additive decomposition and using multiplicative decomposition is the provided perfect tracking to states or to outputs. If the dynamics of the system are clearly modeled and the states of the state-space representation have physical meaning, the approach using additive decomposition is useful because it is clear to which state the perfect tracking is provided. If the dynamics and the physical meaning of the system are not clear and the controller design only focuses on the output, the approach using multiplicative decomposition is useful because it provides the perfect tracking to on-sample output but not to state.

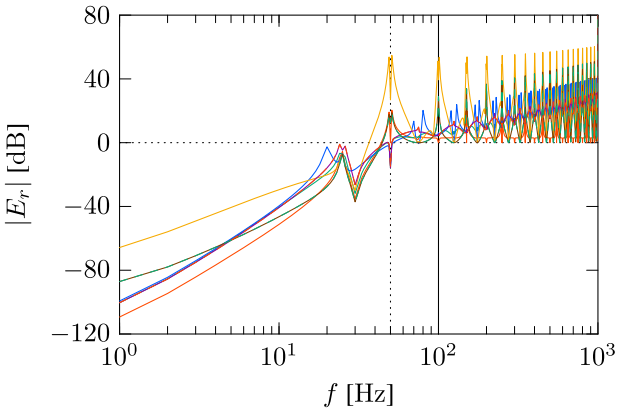

Fig. 6. Performance frequency gain of the continuous-time tracking error in G_c. Vertical lines (····) and (——) show Nyquist frequency $1/2\delta$ and sampling frequency $1/\delta$, respectively. Each line corresponds to 8 approaches from Case 1 to Case 8 in Table 1, respectively.

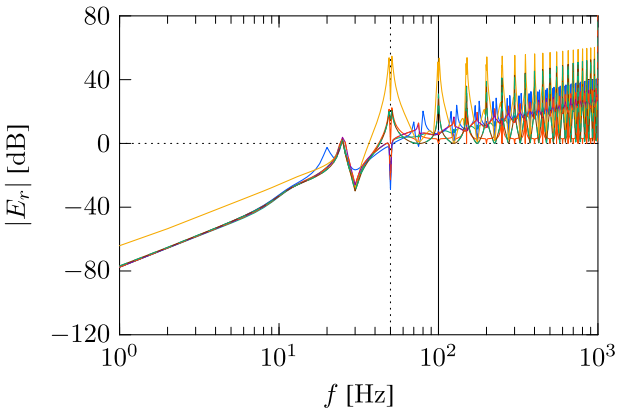

Fig. 7. Performance frequency gain of the continuous-time tracking error in $\hat{G}$. Vertical lines (····) and (——) show Nyquist frequency $1/2\delta$ and sampling frequency $1/\delta$, respectively. Each line corresponds to 8 approaches from Case 1 to Case 8 in Table 1, respectively.

5.2. Frequency domain verification

In frequency domain verification, the intersample performance is verified by the performance frequency gain $|E_r|$ (Fujimoto, 2000; Lindgarde & Lennartson, 1997; Oomen, van de Wal, & Bosgra, 2007) in the simulation that is the steady state continuous-time tracking error normalized by the step sine wave reference and is defined as

$$
|E_r(\mathrm{j}\omega)| = \frac{\mathrm{RMS}(e_{\mathrm{j}\omega}(t))}{\mathrm{RMS}(r_{\mathrm{j}\omega}(t))}, \tag{102}
$$

where $r_{\mathrm{j}\omega}(t)$ can only contain a single frequency at each frequency and the intersample performance is evaluated in the sampling time $\delta/20 = 0.5$ ms.

The performance frequency gain of the continuous-time tracking error in G_c without modeling error is shown in Fig. 6. It shows that Case 5 = Case 7 and Case 6 = Case 8 in the performance frequency gain. It is because the discretization only affects the dynamics of zeros, and the choice of the pole does not affect the performance. Case 4 makes a large error for the whole frequency range because it cannot compensate for rigid body dynamics. The approaches like Case 1, Case 6, and Case 8 that cannot compensate for oscillating poles of the feedforward controller due to discretization make large errors around

Table 1
Comparison of 8 approaches. T_r is the reference sampling time. $G_{c,mr}$ and $G_{c,sr}$ are the continuous-time model for the multirate and single-rate inversion. Intersample performance is evaluated by the Root Mean Square of the tracking error $e_{\mathrm{RMS}} = \mathrm{RMS}(e(t))$ with the sampling time $\delta/20 = 0.5\,\mathrm{ms}$. The evaluations are conducted by the simulation of G_c without feedback control, $\hat{G}$ without feedback control, and $\hat{G}$ with feedback control, and by the experiment.

Case	Line	Approach	T_r	$G_{c,mr}$	$G_{c,sr}$	G_c w/o FB	$\hat{G}$ w/o FB	$\hat{G}$ with FB	Experiment
1	—	Single-rate	δ	–	G_c	9862 nm	16 811 nm	17 642 nm	27 152 nm
2	—	Multirate	4δ	G_c	–	5174 nm	11 646 nm	12 406 nm	15 027 nm
3	—	Additive	2δ	G_1	–	8199 nm	12 176 nm	13 397 nm	17 210 nm
4	—	Additive	2δ	G_2	–	>1 mm	>1 mm	–	–
5	—	Multiplicative	2δ	N_1/D_1	N_2/D_2	9309 nm	11 280 nm	12 510 nm	22 579 nm
6	—	Multiplicative	2δ	N_2/D_1	N_1/D_2	8559 nm	14 547 nm	–	–
7	- -	Multiplicative	2δ	N_1/D_2	N_2/D_1	9309 nm	11 280 nm	–	–
8	- -	Multiplicative	2δ	N_2/D_2	N_1/D_1	8559 nm	14 547 nm	–	–

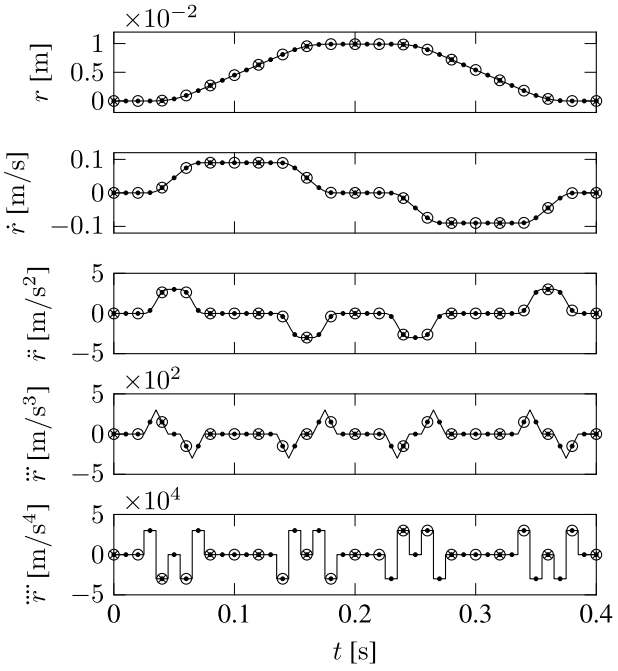

Fig. 8. Continuous-time 4th order polynomial trajectory reference $r(t)$ and its derivatives. (•), (○), and (×) show sampling points every δ, 2δ, and 4δ.

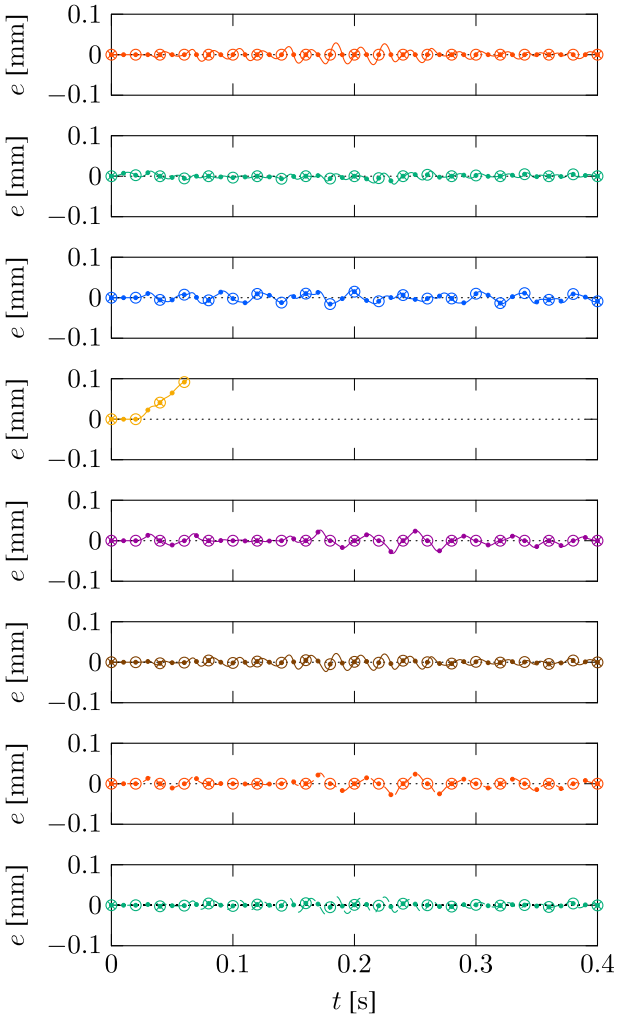

Fig. 9. Error $e(t)$ in the simulation of G_c with sampling time $\delta/20 = 0.5\,\mathrm{ms}$. (•), (○), and (×) show sampling point every δ, 2δ, and 4δ. Each figure from top to bottom corresponds to 8 approaches from Case 1 to Case 8 in Table 1, respectively.

Nyquist frequency. In low frequency, $|E_r|$ is smaller in order of Case 1 < Case 5 = Case 7 < Case 2 < Case 3. From these analyses, Case 2 with multirate feedforward control for full-state tracking provides the best performance in steady state, and Case 2, Case 3, Case 5, and Case 7 are preferable approaches.

The performance frequency gain of the continuous-time tracking error in $\hat{G}$ with modeling error is shown in Fig. 7. There is the same trend around Nyquist frequency compared to the simulation in G_c without modeling error. In low frequency, $|E_r|$ is around the same performance in all approaches except Case 4. It is because the controller cannot compensate for the low-frequency compliance of the unmodeled high-frequency dynamics.

5.3. Time domain verification

In the time domain verification, the intersample performance is verified by the continuous-time tracking error in the simulation for the continuous-time reference trajectory shown in Fig. 8. The intersample performance is evaluated by Root Mean Square error $e_{\mathrm{RMS}} = \mathrm{RMS}(e(t))$ in Table 1 with the sampling time $\delta/20 = 0.5\,\mathrm{ms}$.

The time series error $e(t)$ in G_c without modeling error is shown in Fig. 9. The result shows that Case 2 achieves the best performance because there is no modeling error between the controller and the controlled system and perfect tracking for all states provides smooth intersample behavior.

The time series error $e(t)$ in $\hat{G}$ with modeling error is shown in Fig. 10. The result shows that Case 5 and Case 7 achieve the best performance because the control input contains relatively low-frequency components compared to Case 2, and it does not excite the resonances of the unmodeled dynamics. The performance of Case 1, Case 6, and Case 8 is getting worse in $\hat{G}$ because the oscillating feedforward input due to discretization excites the unmodeled high-frequency dynamics. From these analyses, multirate feedforward control with mode

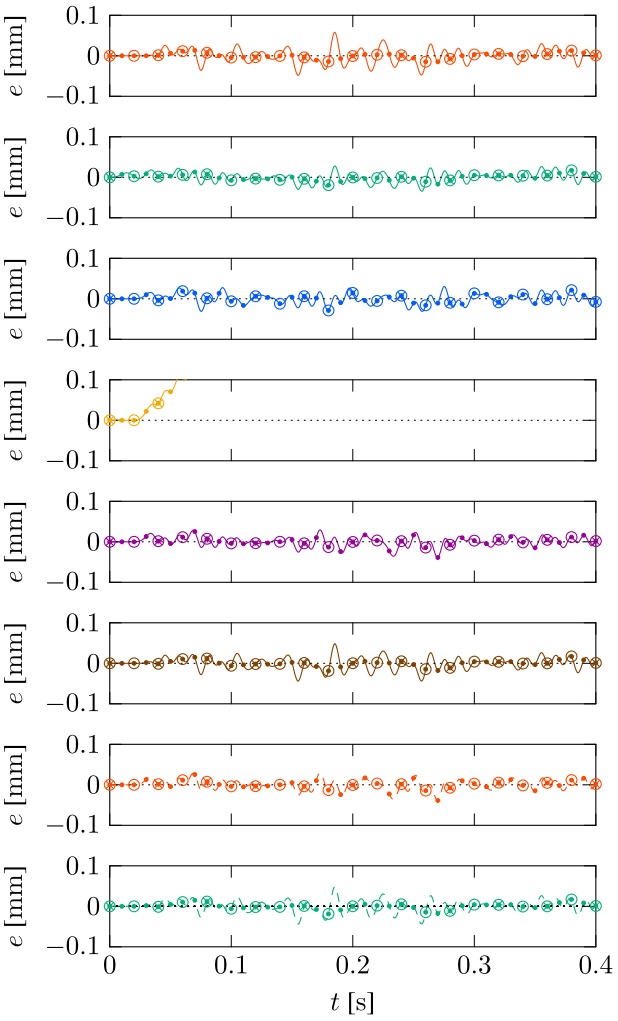

Fig. 10. Error $e(t)$ in the simulation of $\hat{G}$ with sampling time $\delta/20 = 0.5$ ms. (•), (○), and (×) show sampling point every δ, 2δ, and 4δ. Each figure from top to bottom corresponds to 8 approaches from Case 1 to Case 8 in Table 1, respectively.

decomposition can provide better intersample performance in transient response than that of multirate feedforward control for full-state tracking.

5.4. Experimental validation

From the result of the simulation verification, the experimental validation is conducted in Case 1, Case 2, Case 3, and Case 5 as shown in Table 1 with the same reference that is shown in Fig. 8. The overview of the experimental validation is shown in Fig. 11. A feedback controller K is used for stabilization and compensation for low-frequency modeling errors in the experimental validation. For the feedback controller, the PD controller is designed as 5 Hz bandwidth and 6 dB modulus margin. In the two-degree-of-freedom control structure, the feedforward controller handles tracking performance, and the feedback controller handles modeling error and disturbance rejection, independently. As shown in Fig. 11, the feedback controller compensates for the modeling error and disturbance in low frequency. The simulation with the feedback controller and the quantization of the linear encoder is also conducted for the validation of the experimental results.

The time series error $e(t)$ in the experiment is shown in Fig. 12. The result has a similar trend to that in the simulation of $\hat{G}$ with feedback

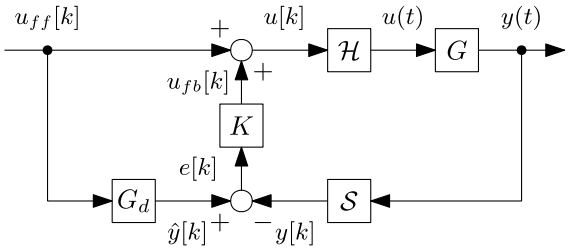

Fig. 11. Block diagram of the experimental validation. G, G_d, K, $\mathcal{S}$ and $\mathcal{H}$ denote a controlled system, a low-order discrete-time model for controller design, a feedback controller, sampler and zero-order-hold, respectively.

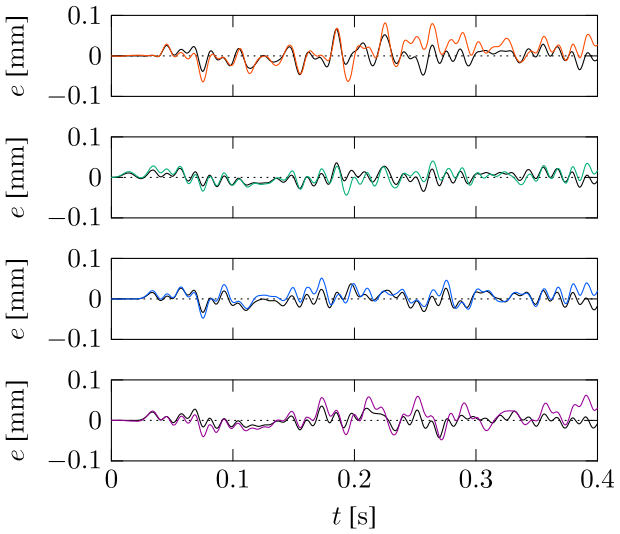

Fig. 12. Error $e(t)$ in the experiment with sampling time $\delta/20 = 0.5$ ms. The solid black line shows that in the simulation of $\hat{G}$ with feedback control. Each figure from top to bottom corresponds to Case 1, 2, 3, and 5 in Table 1, respectively.

control. Note that due to experimental conditions such as model mismatches, the exact on-sample tracking is not provided. The intersample performance is evaluated by Root Mean Square error $e_{\mathrm{RMS}} = \mathrm{RMS}(e(t))$ in Table 1 with the sampling time $\delta/20 = 0.5$ ms. It shows that Case 2 with multirate feedforward control for full-state tracking provides the best performance in simulation and experiment with feedback control. The amplitude spectrum of error $e(t)$ in the experiment is shown in Fig. 13. The result shows that Case 1 and Case 5 which contain single-rate filters have a large error in over sampling frequency because the frequency components of the feedforward input over sampling frequency excite the unmodeled high-frequency dynamics.

6. Conclusion

In this paper, perfect tracking control approaches are described focusing on intersample performance in multi-modal motion systems. The model of the multi-modal motion system is decomposed into combinations of the states that can be selected for the perfect tracking control. The simulation verification and experimental validation in a multi-modal motion system show that state tracking should be used to compensate for the oscillating poles of the feedforward controller due to discretization. In summary, the feedforward controller to improve intersample performance should be designed with the following conditions.

- State tracking approach with lifted samples at least the same number as the relative degree can compensate for oscillating poles of the feedforward controller due to discretization when the relative degree of the continuous-time model is 2 or more.

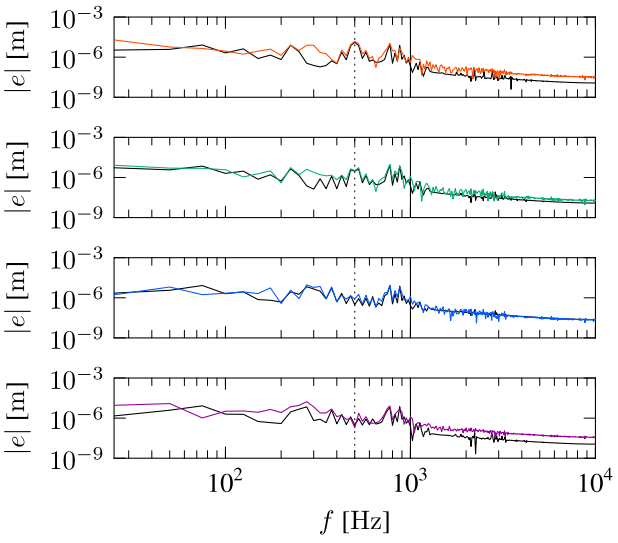

Fig. 13. Amplitude spectrum of error $e(t)$ in the experiment with sampling time $\delta/20 = 0.5$ ms. The solid black line shows that in the simulation of $\hat{G}$ with feedback control. Vertical lines (····) and (——) show Nyquist frequency $1/2\delta$ and sampling frequency $1/\delta$, respectively. Each figure from top to bottom corresponds to Case 1, 2, 3, and 5 in Table 1, respectively.

- For steady-state performance without modeling error, multirate feedforward control for full-state tracking provides the best performance.
- Multirate feedforward control with mode decomposition can provide the best intersample performance in transient response depending on the frequency components of the reference and the unmodeled dynamics of the controlled system.

Ongoing research focuses on the optimal mode selection depending on the reference signal in higher-order motion systems.

Declaration of competing interest

The authors declare that they have no known competing financial interests or personal relationships that could have appeared to influence the work reported in this paper.

Acknowledgment

This research is supported by JSPS KAKENHI Grant Number 21J13196.

References

Åström, K. J., Hagander, P., & Sternby, J. (1984). Zeros of sampled systems. *Automatica: The Journal of IFAC, the International Federation of Automatic Control*, *20*(1), 31–38.

Butterworth, J. A., Pao, L. Y., & Abramovitch, D. Y. (2012). Analysis and comparison of three discrete-time feedforward model-inverse control techniques for nonminimum-phase systems. *Mechatronics: The Science of Intelligent Machines*, *22*(5), 577–587.

Chen, T., & Francis, B. A. (1995). *Optimal sampled-data control systems*. London: Springer London.

Duan, M., Yoon, D., & Okwudire, C. E. (2018). A limited-preview filtered B-spline approach to tracking control – With application to vibration-induced error compensation of a 3D printer. *Mechatronics: the Science of Intelligent Machines*, *56*, 287–296.

Fujimoto, H. (2000). *General framework of multirate sampling control and applications to motion control systems* (Ph.D. thesis), The University of Tokyo.

Fujimoto, H., Hori, Y., & Kawamura, A. (2001). Perfect tracking control based on multirate feedforward control with generalized sampling periods. *IEEE Transactions on Industrial Electronics*, *48*(3), 636–644.

Gawronski, W. (2004). *Advanced structural dynamics and active control of structures*. New York: Springer Science & Business Media.

Gross, E., Tomizuka, M., & Messner, W. (1994). Cancellation of discrete time unstable zeros by feedforward control. *Journal of Dynamic Systems, Measurement, and Control*, *116*(1), 33–38.

Hayashi, T., Fujimoto, H., Isaoka, Y., & Terada, Y. (2020). Projection-based iterative learning control for ball-screw-driven stage with consideration of rolling friction compensation. *IEEJ Journal of Industry Applications*, *9*(2), 132–139.

Hirata, M., & Ueno, F. (2011). Final-state control using polynomial and time-series data. *IEEE Transactions on Magnetics*, *47*(7), 1944–1950.

Lindgarde, O., & Lennartson, B. (1997). Performance and robust frequency response for multirate sampled-data systems. *Vol. 6*, In *1997 American control conference (ACC)* (pp. 3877–3881). IEEE.

Mae, M., Ohnishi, W., & Fujimoto, H. (2019). State trajectory generation for MIMO multirate feedforward using singular value decomposition and time axis reversal. *2019-July*, In *2019 American control conference (ACC)* (pp. 5693–5698). IEEE.

Mae, M., Ohnishi, W., & Fujimoto, H. (2020). MIMO multirate feedforward controller design with selection of input multiplicities and intersample behavior analysis. *Mechatronics: The Science of Intelligent Machines*, *71*(February), Article 102442.

Mae, M., Ohnishi, W., & Fujimoto, H. (2021). Multirate feedforward control based on modal form with mode selection applied to multi-modal high-precision positioning stage. In *2021 IEEE international conference on mechatronics (ICM)* (pp. 1–6). IEEE.

Ohnishi, W., Beauduin, T., & Fujimoto, H. (2019). Preactuated multirate feedforward control for independent stable inversion of unstable intrinsic and discretization zeros. *IEEE/ASME Transactions on Mechatronics*, *24*(2), 863–871.

Ohnishi, W., & Fujimoto, H. (2018). Multirate feedforward control based on modal form. In *2018 IEEE conference on control technology and applications (CCTA)* (pp. 1120–1125). IEEE.

Oomen, T., van de Wal, M., & Bosgra, O. (2007). Design framework for high-performance optimal sampled-data control with application to a wafer stage. *International Journal of Control*, *80*(6), 919–934.

Poot, M., Portegies, J., Mooren, N., van Haren, M., van Meer, M., & Oomen, T. (2022). Gaussian processes for advanced motion control. *IEEJ Journal of Industry Applications*, *11*(3), 396–407.

Skogestad, S., & Postlethwaite, I. (2005). *Multivariable feedback control* (2nd ed.). John Wiley & Sons, Ltd.

Steinbuch, M., Oomen, T., & Vermeulen, H. (2021). Motion control, mechatronics design, and Moore's law. *IEEJ Journal of Industry Applications*, *2*(4), Article 21006010.

Tomizuka, M. (1987). Zero phase error tracking algorithm for digital control. *Journal of Dynamic Systems, Measurement, and Control*, *109*(1), 65.

Totani, T., & Nishimura, H. (1994). Final-state control using compensation input. *Transactions of the Society of Instrument and Control Engineers*, *30*(3), 253–260.

Voorhoeve, R., de Rozario, R., Aangenent, W., & Oomen, T. (2021). Identifying position-dependent mechanical systems: A modal approach applied to a flexible wafer stage. *IEEE Transactions on Control Systems Technology*, *29*(1), 194–206.

Wen, J. T., & Potsaid, B. (2004). An experimental study of a high performance motion control system. *Vol. 6*, In *2004 American control conference (ACC)* (pp. 5158–5163). IEEE.

van Zundert, J., Luijten, F., & Oomen, T. (2019). Exact and causal inversion of nonminimum-phase systems: A squaring-down approach for overactuated systems. *IEEE/ASME Transactions on Mechatronics*, *24*(6), 2953–2963.

van Zundert, J., Ohnishi, W., Fujimoto, H., & Oomen, T. (2020). Improving intersample behavior in discrete-time system inversion: With application to LTI and LPTV systems. *IEEE/ASME Transactions on Mechatronics*, *25*(1), 55–65.

van Zundert, J., & Oomen, T. (2018). On inversion-based approaches for feedforward and ILC. *Mechatronics: the science of intelligent machines*, *50*(vember 2016), 282–291.